Fast algorithm for scaling analysis with higher-order detrending moving average method

Yutaka Tsujimoto, Yuki Miki, Satoshi Shimatani, and Ken Kiyono*
Graduate School of Engineering Science, Osaka University, 1-3 Machikaneyama-cho, Toyonaka, Osaka 560-8531, Japan
(Received 3 February 2016; published 16 May 2016)

Among scaling analysis methods based on the root-mean-square deviation from the estimated trend, it has been demonstrated that centered detrending moving average (DMA) analysis with a simple moving average has good performance when characterizing long-range correlation or fractal scaling behavior. Furthermore, higher-order DMA has also been proposed; it is shown to have better detrending capabilities, removing higher-order polynomial trends than original DMA. However, a straightforward implementation of higher-order DMA requires a very high computational cost, which would prevent practical use of this method. To solve this issue, in this study, we introduce a fast algorithm for higher-order DMA, which consists of two techniques: (1) parallel translation of moving averaging windows by a fixed interval; (2) recurrence formulas for the calculation of summations. Our algorithm can significantly reduce computational cost. Monte Carlo experiments show that the computational time of our algorithm is approximately proportional to the data length, although that of the conventional algorithm is proportional to the square of the data length. The efficiency of our algorithm is also shown by a systematic study of the performance of higher-order DMA, such as the range of detectable scaling exponents and detrending capability for removing polynomial trends. In addition, through the analysis of heart-rate variability time series, we discuss possible applications of higher-order DMA.

DOI: 10.1103/PhysRevE.93.053304

I. INTRODUCTION

Long-range correlations and fractal scaling behavior of time series have been observed in a wide variety of systems, including biological [1–6], economic [7–9], and social systems [10,11]. Understanding these dynamics has become a major concern in the field of complex and far-from-equilibrium systems [12,13]. In addition, recent advances in computing, communications, and digital storage technologies have led to the generation of large-scale, high-frequency data [14]. Analysis of this large-scale data would also be important to obtain insight into the mechanisms underlying long-range correlations in real-world systems. Furthermore, using wearable devices for medical and healthcare applications, it is possible to record very long-term, continuous biomedical signals [15,16] such as electrocardiograms, heart rate, blood pressure, blood oxygen saturation, body temperature, posture, and physical activity. In biomedical time series, long-range correlation has frequently been observed [1–3,5,17]. The importance of characterizing the long-range correlation in biomedical time series is underscored by studies demonstrating that its alteration is associated with a disease state and higher mortality [5,16–18]. Thus, fast and reliable characterization of a large-scale time series dataset is a crucial task.

To quantify the long-range correlation, a variety of techniques have been proposed, such as power spectral analysis [19], rescaled range (R/S) analysis [20], structure-function-based analysis [21], wavelet-transform-based analysis [22–24], detrended fluctuation analysis (DFA) [3,4,25], and detrending moving average (DMA) algorithms [8,26–28]. As in DFA and DMA, one possible method of characterizing a stochastic process exhibiting fractal scaling behavior, such as fractional Brownian motion [29], is to estimate the power-law increase ($\sim n^{\alpha}$) in the root-mean-square deviation from a trend, as the observation window size n increases. In this approach, the power-law exponent α, called the scaling exponent, is expected to provide an estimate of the Hurst exponent H of fractional Brownian motion [29]. If we observe a long-range correlated time series displaying nondiffusive behavior, such as fractional Gaussian noise (fGn) [29], we analyze its integrated series (cumulative sum) as a sample path of a random walk driven by the observed time series. In this case, long-range correlation properties of the observed time series are characterized by the scaling exponent α.

To achieve reliable detection of the scaling behavior in nonstationary time series with trends, it is essential to distinguish deterministic trends from the long-range correlation intrinsic in the stochastic dynamics. Therefore, various types of detrending procedures used to minimize the effects of trends have been introduced in scaling analysis [6,26,27,30–33]. Among these methods, centered DMA [8] is one of the best performing methods [31,34], although its detrending ability is worse than that of second-order DFA [35]. In DMA, the trend is estimated using a simple moving average [8,26–28]. As a generalization of DMA, higher-order DMA has also been proposed [33]. In higher-order DMA, a higher order moving average, defined based on a moving average polynomial of degree m, is employed as the estimated trend (Fig. 1). If moving average polynomials of degree m are employed in the DMA, the method is referred to as mth order DMA or DMA$_m$. In this framework, the original DMA is included as the zeroth order DMA (DMA$_0$). Recently, it has been analytically shown that higher-order DMA has a better detrending capability for removing a higher-order polynomial trend [36]. In practical applications, to analyze nonstationary time series with an *a priori* unknown trend, the higher detrending capability is important for improving the estimation accuracy and validating the observed scaling behavior [25,31]. However, the

*kiyono@bpe.es.osaka-u.ac.jp

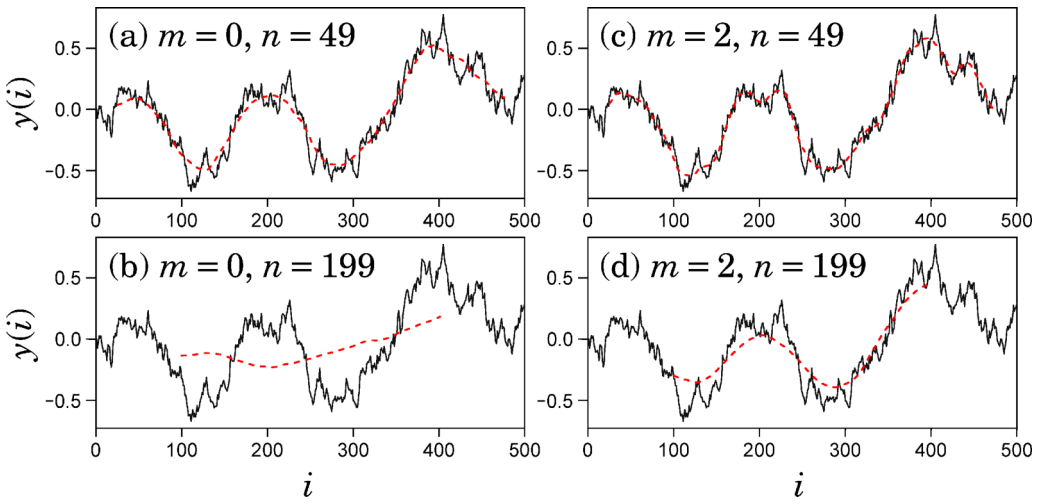

FIG. 1. Moving average polynomials $\{\tilde{y}_n(i)\}$ of degree m at scale n (dashed lines) in centered DMA, where $\{y(i)\}$ is a discrete sample path of Brownian motion.

implementation of higher-order DMA significantly increases the computational cost. Although this fact has not been explicitly identified, it is likely the main reason why no systematic and comprehensive study based on Monte Carlo experiments has been conducted to investigate the performance of higher-order DMA.

In this paper, to reduce the computational cost of higher-order DMA, we propose a fast algorithm. Monte Carlo experiments show that the computational time of our algorithm is approximately proportional to N, where N is the data length, whereas that of the conventional algorithm is approximately proportional to N^2. The efficiency of our algorithm is also shown using a systematic study of the performance of higher-order DMA, such as the order dependence of the detectable scaling exponent and detrending capability for removing a polynomial trend. In addition, as an application of our method, we analyze heart-rate variability (HRV) time series obtained from the Physionet database [37].

The organization of this paper is as follows. In Sec. II, we describe the higher-order DMA. In Sec. III, we propose a first algorithm for DMA, and demonstrate the efficiency of our algorithm. In Sec. IV, based on Monte Carlo experiments, we test the performance of our algorithm and higher-order DMA. In Sec. V, through the analysis of HRV, we evaluate possible applications of higher-order DMA. Finally, Sec. VI provides a summary of our results and discusses possible extensions of our algorithm.

II. DETRENDING MOVING AVERAGE (DMA) ALGORITHM

In this section, we briefly review higher-order DMA. To analyze a long-range correlated time series displaying nondiffusive behavior, we first integrate the observed time series $\{x(i)\}_{i=1}^{N}$, $y(i) = \sum_{j=1}^{i} [x(j) - \overline{x}\,]$, where $\overline{x}$ is the sample mean of $\{x(i)\}$, and analyze $\{y(i)\}$. In the DMA algorithm, to obtain a moving average polynomial of degree m, we consider a least-squares polynomial fit for a moving window of length n. In this case, the coefficients $\{\tilde{a}_{n,k}\}$ of the mth order polynomial fit, i.e., $\tilde{a}_{n,0}(i) + \tilde{a}_{n,1}(i)\, i + \cdots + \tilde{a}_{n,m}(i)\, i^m$, are given by

$$\begin{bmatrix} \tilde{a}_{n,0}(i) \\ \tilde{a}_{n,1}(i) \\ \vdots \\ \tilde{a}_{n,m}(i) \end{bmatrix} = B_m^{-1}(i,n) \begin{bmatrix} \sum_j y(j) \\ \sum_j j\, y(j) \\ \vdots \\ \sum_j j^m y(j) \end{bmatrix}, \tag{1}$$

where $B_m^{-1}(i,n)$ is the inverse matrix of

$$B_m(i,n) = \begin{bmatrix} \sum_j 1 & \sum_j j & \cdots & \sum_j j^m \\ \sum_j j & \sum_j j^2 & \cdots & \sum_j j^{m+1} \\ \vdots & \vdots & \ddots & \vdots \\ \sum_j j^m & \sum_j j^{m+1} & \cdots & \sum_j j^{2m} \end{bmatrix}. \tag{2}$$

The range of the summations in Eqs. (1) and (2) depends on time (or position) i, the relative location of the moving average point, and the moving window size n. In centered DMA, the summations are calculated over $[i - (n-1)/2, i + (n-1)/2]$, where we assume that n is an odd number. In forward DMA, summations are over $[i, i+n-1]$. In backward DMA, summations are over $[i-n+1, i]$. Using $\{\tilde{a}_{n,k}(i)\}$ [Eq. (1)], the moving average polynomial of degree m $\{\tilde{y}_n(i)\}$ is given by

$$\tilde{y}_n(i) = \tilde{a}_{n,0}(i) + \tilde{a}_{n,1}(i)\, i + \cdots + \tilde{a}_{n,m}(i)\, i^m. \tag{3}$$

An illustrative example of moving average polynomials in centered DMA is shown in Fig. 1. The above definition of the moving average polynomial using Eqs. (1)–(3) is based on the original procedure proposed in Ref. [33]. However, as will be shown later, the moving average polynomial can be presented in a more sophisticated form. In this study, it is shown that the moving average polynomial [Eq. (3)] is a linear function (filter) of $\{y(i)\}$ and does not explicitly depend on i. For example, in

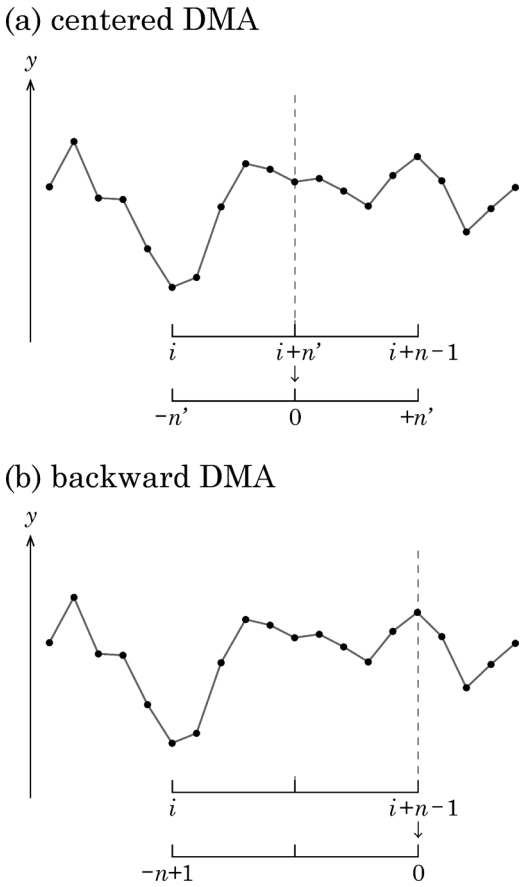

FIG. 2. Illustration of parallel translation of a moving averaging window. In centered DMA, each moving average window over $[i,i+n-1]$ is shifted by a fixed interval $[-n',n']$, where n is the window size and $n=2n'+1$. In backward DMA, each moving average window over $[i,i+n-1]$ is shifted by a fixed interval $[-n+1,0]$.

second-order centered DMA at odd scale n, $\tilde{y}_n(i)$ is given by

$$\tilde{y}_n(i) = \frac{9n^2-21}{4n^3-16n}\sum_{j=-(n-1)/2}^{(n-1)/2} y[i+j] - \frac{15}{n^3-4n}\sum_{j=-(n-1)/2}^{(n-1)/2} j^2\, y[i+j], \qquad (4)$$

where i and i^2 are not explicitly included [cf. Eq. (3)].

Using the estimated trend $\{\tilde{y}_n(i)\}$, an estimator of the mean-square deviation from the trend, called the generalized variance, can be defined as

$$\sigma^2_{\mathrm{DMA}}(n) = \frac{1}{N-n}\sum_i [y(i)-\tilde{y}_n(i)]^2, \qquad (5)$$

where N is the data length, and the range of the summation depends on both the analyzed scale n and the type of DMA. In centered DMA, the summations are calculated over $[1+(n-1)/2, N-(n-1)/2]$ for odd values of n. In forward DMA, summation is over $[1, N-(n-1)]$. In backward DMA, summation is over $[n,N]$. In the original definition of the generalized variance [Eq. (5)], the denominator is set to $(N-n)$ [27]. However, to maintain consistency between our analytical and numerical arguments throughout this paper, we replace $(N-n)$ by $(N-n+1)$ in Eq. (5). Note that the asymptotic behavior is the same in both cases.

In Eq. (1), the calculation steps of summations of $\{y(i)\}$ are proportional to $n(N-n+1)\sim nN$. In the scaling analysis, the analyzed scales are given by a finite sequence $\{n_1,n_2,\ldots,n_L\}$, where L is the number of analyzed scales. If $\{n_l\}_{l=1}^{L}$ is given by a geometric progression with a fixed common ratio and the last term proportional to the data length N, the sum of $\{n_l\}$ is proportional to N. Therefore, the total number of steps in the summations in Eq. (1) is approximately proportional to N^2, which means that the computation time rapidly increases as the data length N increases.

III. FAST ALGORITHM FOR DMA

To reduce the computational cost of higher-order DMA, here we propose a fast algorithm. Our approach to developing a fast algorithm for DMA consists of two principles: (1) parallel translation of moving averaging windows by a fixed interval (Fig. 2); (2) recurrence formulas for the calculation of summations (Fig. 3). The parallel translation of the moving averaging windows has two advantages. One advantage is that $B_m^{-1}(i,n)$ in Eq. (1) at each scale n is calculated only once, not repeatedly. The other advantage is that the moving average polynomial $\tilde{y}_n(i)$ [Eq. (3)] is always simplified as follows:

$$\tilde{y}_n(0) = \tilde{a}_{n,0}(0) + \tilde{a}_{n,1}(0)0 + \cdots + \tilde{a}_{n,m}(0)0^m = \tilde{a}_{n,0}(0).$$

Thus, it is not necessary to calculate the coefficients of higher-order terms in Eq. (3). Using this idea, we can derive simplified forms of the calculation procedure corresponding to

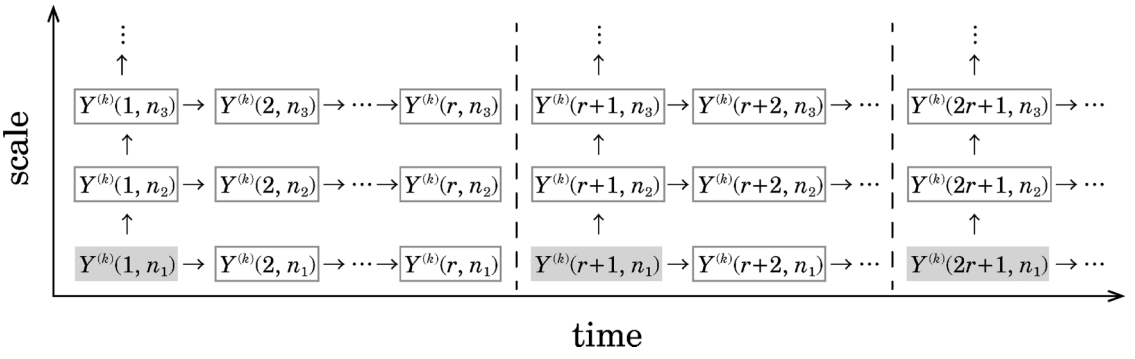

FIG. 3. Illustration of recurrence calculations of $Y^{(k)}(i,n)$. Every r point in the smallest scale n_1, $Y^{(k)}(lr+1,n_1)$ $(l=0,1,\cdots)$ is calculated using $\sum_j j^k\, y(j)$ (gray shaded terms). Otherwise, subsequent $Y^{(k)}(i,n)$ values are calculated using recurrence formulas.

Eqs. (1)–(3). For example, in centered DMA with even-order m, the moving average polynomial $\tilde{y}_n(i)$ of degree m at odd scale n is given by

$$\tilde{y}_n(i) = \sum_{k=0}^{m/2} \left(\tilde{b}_{1,2k+1}(n) \sum_{j=-(n-1)/2}^{(n-1)/2} j^{2k}\, y[i+j] \right), \quad (6)$$

where $\tilde{b}_{i,j}(n)$ are elements of the $(m+1)\times(m+1)$ matrix $\tilde{B}_m^{-1}(n)$, where $\tilde{B}_m^{-1}(n)$ is the inverse matrix of

$$\tilde{B}_m(n) = \sum_{j=-(n-1)/2}^{(n-1)/2} \begin{bmatrix} 1 & 0 & j^2 & \cdots & j^m \\ 0 & j^2 & 0 & \cdots & 0 \\ j^2 & 0 & j^4 & \cdots & j^{m+2} \\ \vdots & \vdots & \vdots & \ddots & \vdots \\ j^m & 0 & j^{m+2} & \cdots & j^{2m} \end{bmatrix}. \quad (7)$$

In DMA, the calculation of $\sum_j j^k y(j)$ in Eq. (1) [or Eq. (6)] results in a high computational cost. In our algorithm, by introducing recurrence formulas to calculate $\sum_j j^k y(j)$, the computational cost is reduced. As will be shown, the summations can be recurrently calculated across both time i and analyzed scales. However, iterative calculations of the recurrence formulas in the computer will cause rounding errors to accumulate. To minimize this rounding error accumulation, we introduce a refresh interval r, where r is a positive integer. In our algorithm, calculations of $\sum_j j^k y(j)$ at every r point in the smallest scale are straightforwardly carried out, without using the recurrence formulas (Fig. 3). In the following subsection, we provide the details of the algorithm for centered DMA. The algorithm for backward DMA is provided in Appendix A.

A. Algorithm for centered DMA

In our algorithm for the centered case, the description of DMA with even order m is exactly the same as that for $(m+1)$th order DMA. Therefore, here we consider even order DMA. In this case, the mean-square deviation from the trend at scale $n = 2n'+1$, where n' is a positive integer, is given by

$$\sigma^2_{\mathrm{DMA}}(n) = \frac{1}{N-2n'} \sum_{i=1}^{N-2n'} [y(i+n') - \tilde{a}_{n,0}(i)]^2, \quad (8)$$

where N is the data length and $\tilde{a}_{n,0}(i)$ is given by

$$\begin{aligned} \tilde{a}_{n,0}(i) &= \tilde{b}_{1,1}\, Y^{(0)}(i,n') + \tilde{b}_{1,3}\, Y^{(2)}(i,n') \\ &\quad + \cdots + \tilde{b}_{1,m+1}\, Y^{(m)}(i,n') \\ &= \sum_{k=0}^{m/2} \tilde{b}_{1,2k+1}\, Y^{(2k)}(i,n'). \end{aligned} \quad (9)$$

In Eq. (9), $Y^{(k)}(i,n')$ is defined by

$$Y^{(k)}(i,n') = \sum_{j=1}^{2n'+1} (j-n'-1)^k\, y(i+j-1), \quad (10)$$

and $\tilde{b}_{i,j}$ defines elements of the $(m+1)\times(m+1)$ matrix $\tilde{B}_m^{-1}(n')$, where $\tilde{B}_m^{-1}(n')$ is the inverse matrix of

$$\tilde{B}_m(n') = \sum_{j=-n'}^{n'} \begin{bmatrix} 1 & 0 & j^2 & \cdots & j^m \\ 0 & j^2 & 0 & \cdots & 0 \\ j^2 & 0 & j^4 & \cdots & j^{m+2} \\ \vdots & \vdots & \vdots & \ddots & \vdots \\ j^m & 0 & j^{m+2} & \cdots & j^{2m} \end{bmatrix}. \quad (11)$$

We would like to point out that moving average polynomials of higher-order centered DMA are identical with Savitzky-Golay filters [38,39].

In our algorithm, if the condition $i = ri'+1$ is satisfied, where $i' = 0,1,\ldots,\lfloor (N-1)/r \rfloor$ ($\lfloor\cdot\rfloor$ is the floor function) and the refresh interval r is a positive integer, $Y^{(k)}(i,n'_1)$ at the smallest scale n'_1 is straightforwardly calculated using Eq. (10). Otherwise, subsequent $Y^{(k)}(i,n'_l)$ values are calculated using recurrence formulas:

$$\begin{aligned} Y^{(k)}(i+1,n'_l) &= \sum_{j=0}^{k} \binom{k}{j} (-1)^{k-j}\, Y^{(j)}(i,n'_l) \\ &\quad -(-n'_l-1)^k\, y(i) + (n'_l)^k\, y(i+2n'_l+1). \end{aligned} \quad (12)$$

In addition, the relation between the two scales, i.e., n'_l and n'_{l+1}, is given by

$$\begin{aligned} Y^{(k)}(i,n'_{l+1}) &= \sum_{j=0}^{k} \binom{k}{j} (n'_l - n'_{l+1})^{k-j}\, Y^{(j)}(i,n'_l) \\ &\quad + \sum_{j=2n'_l+2}^{2n'_{l+1}+1} (j-n'_{l+1}-1)^k\, y(i+j-1). \end{aligned} \quad (13)$$

If the two conditions, i.e., $n'_l > n'_1$ and $i = ri'+1$, are satisfied, $Y^{(k)}(i,n'_l)$ is calculated using Eq. (13).

For example, in second-order centered DMA, $\sigma^2_{\mathrm{DMA}}(n)$ at scale $n = 2n'+1$ is given by

$$\sigma^2_{\mathrm{DMA}}(2n'+1) = \frac{1}{N-2n'} \sum_{i=1}^{N-2n'} \left[y(i+n') - \frac{(9n'^2+9n'-3)Y^{(0)}(i,n') - 15Y^{(2)}(i,n')}{8n'^3+12n'^2-2n'+3} \right]^2. \quad (14)$$

In this case, the recurrence formulas for the calculation of $Y^{(k)}(i,n'_l)$ values are given by

$$Y^{(0)}(i+1,n') = Y^{(0)}(i,n') + y(i+2n'+1) - y(i), \quad (15)$$

$$Y^{(1)}(i+1,n') = Y^{(1)}(i,n') - Y^{(0)}(i,n') + (n'+1)y(i) + n'\, y(i+2n'+1), \quad (16)$$

$$Y^{(2)}(i+1,n') = Y^{(2)}(i,n') - 2Y^{(1)}(i,n') + Y^{(0)}(i,n') - (n'+1)^2 y(i) + n'^2\, y(i+2n'+1). \quad (17)$$

In addition, when $n'_l > n'_1$ and $i = ri' + 1$, the values of $Y^{(k)}(i,n'_l)$ are calculated as follows:

$$Y^{(0)}(i,n'_{l+1}) = Y^{(0)}(i,n'_l) + \sum_{j=2n'_l+2}^{2n'_{l+1}+1} y(i+j-1), \tag{18}$$

$$Y^{(1)}(i,n'_{l+1}) = Y^{(1)}(i,n'_l) + (n'_l - n'_{l+1})\,Y^{(0)}(i,n'_l) + \sum_{j=2n'_l+2}^{2n'_{l+1}+1} (j - n'_{l+1} - 1)\,y(i+j-1), \tag{19}$$

$$Y^{(2)}(i,n'_{l+1}) = Y^{(2)}(i,n'_l) + 2(n'_l - n'_{l+1})\,Y^{(1)}(i,n'_l) + (n'_l - n'_{l+1})^2\,Y^{(0)}(i,n'_l) + \sum_{j=2n'_l+2}^{2n'_{l+1}+1} (j - n'_{l+1} - 1)^2\,y(i+j-1). \tag{20}$$

B. Setting of refresh interval

To obtain an accurate and fast analysis method, optimization of the refresh interval r is crucial. To determine the value of r, we evaluate the effect of the rounding error accumulation induced by recurrence formulas. Figure 3 shows the relative error induced by iterative calculations of the recurrence formulas [Eq. (12)], where the relative error is defined as the absolute difference between the two methods, i.e., with and without recurrence formulas, divided by the root-mean-square deviation $\sigma_{\mathrm{DMA}}(n)$ of the method without recurrence formulas. As shown in Fig. 4, the relative error rapidly increases as the number of iterations increases. To achieve a sufficiently small relative error, i.e., less than 10^{-5}, we set $r = 10^4$ for centered DMA_2 and $r = 100$ for centered DMA_4 in the following analysis. In addition, we set $r = 10^5$ for centered DMA_0, backward DMA_0, and backward DMA_1; $r = 10^4$ for backward DMA_2; $r = 10^3$ for backward DMA_3; and $r = 10^2$ for backward DMA_4.

C. Comparison of computation times

To evaluate the efficiency of our algorithm, here we estimate the computation time of DMA when combined with DFA [25] via Monte Carlo experiments. DFA was performed based on the original C code available on PhysioNet at http://physionet.org/physiotools/dfa. Here, the analyzed scales $\{n_l\}$ are the odd integers nearest to the geometric progression with a common ratio of $2^{1/8}$. Thus, the number of the analyzed scales is approximately proportional to $\log N$, where N is the data length.

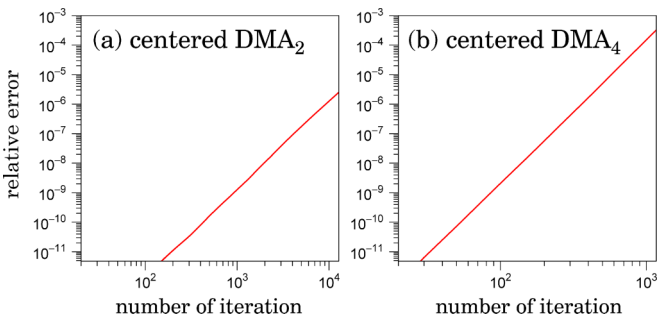

FIG. 4. Relative error induced by iterative calculations of recurrence formulas [Eq. (12)]. The relative error is defined in the text. The mean values of the relative error when $n = 11$ were calculated using 100 samples of white Gaussian noise.

As shown in Fig. 5, the straightforward implementation of DMA provokes a much higher computational cost that is approximately proportional to N^2. In contrast, the computation time of our DMA algorithm is approximately proportional to N^1. In addition, when the mth order centered DMA is compared to the $(m+1)$th order DFA as a comparable method [36], the computation time of DMA is comparable to (or slightly better than) that of DFA.

IV. NUMERICAL STUDY OF HIGHER-ORDER DMA

To date, there are few numerical studies of the performance of higher-order DMA [33,36]. In this study, using analysis of the basic properties of higher-order DMA (such as the range of detectable scaling exponents and detrending capability for removing a polynomial trend), we discuss the efficiency of our algorithm.

A. Limit of detectable scaling exponent

In this section, we investigate the scaling exponent detectable by centered DMA and backward DMA when applied

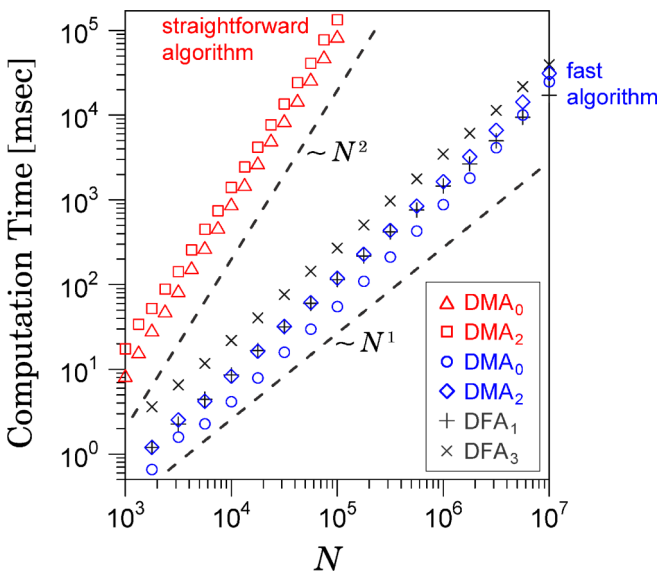

FIG. 5. Comparison of computation times. The CPU time of the process calculating $\sigma_{\mathrm{DMA}}(n)$ were measured on a Windows PC with an Intel Core i7-5930K (3.5 GHz). The computation times were averaged over 100 runs.

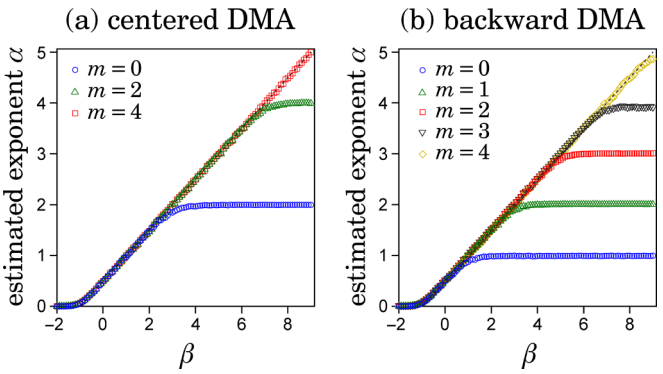

FIG. 6. Estimated scaling exponent α for mth order DMA versus the scaling exponent β of the analyzed time series. Numerically generated time series displaying the power-law scaling of the power spectral density, $S(f) \sim f^{-\beta}$, were analyzed. The length of the time series is $N = 10^5$. The mean value of α, estimated using linear regression of $\log_{10} \sigma_{\mathrm{DMA}}(n)$ versus $\log_{10} n$ in the range $10^2 \leqslant n \leqslant 10^4$, was calculated based on 10 samples. Dashed lines represent the relation $\alpha = (\beta + 1)/2$.

to artificially generated signals with a power-law power spectral density, $S(f) \sim f^{-\beta}$, where f is the frequency. The relation between α and β of these signals is expected to obey $\alpha = (\beta + 1)/2$ [36]. However, it is known that, depending on the analysis method, a limitation of the detectable scaling exponent exists [36,40].

In our analysis, we vary β over $-2 \leqslant \beta \leqslant 9$, and estimate the exponent α in the scaling range $[10^2, 10^4]$. As shown in Fig. 6, the upper limit of the detectable scaling exponent depends on the order of DMA. As predicted by an analytical calculation based on the single-frequency response function, in the case of centered DMA with even order m, the upper limit of α is given by $m + 2$ [36]. On the other hand, in the case of backward DMA with order m, the upper limit of α is given by $m + 1$, which is also predicted using the structure of the single-frequency response function (see Appendix B). Because the single-frequency response function of mth order forward DMA is the same as that of mth order backward DMA, the upper limit of α in forward DMA is the same as that in backward DMA.

To obtain the numerical results shown in Fig. 6(a), the time series of length 10^5 was analyzed 1100 times for each DMA method. Using our algorithm, the total computational time for calculating $\sigma_{\mathrm{DMA}}(n)$ in DMA_0, DMA_2, and DMA_4 was roughly 53 s, 112 s, and 12 min, respectively, excluding the time required to generate and read the data. In contrast, if we use the straightforward algorithm to obtain the same results, the estimated computational time in DMA_0, DMA_2, and DMA_4 was 26 h, 43 h, and 90 h, respectively. Without using our algorithm, the Monte Carlo study of higher-order DMA requires considerable computational costs.

B. Detrending capability

One advantage of higher-order DMA is better detrending performance, which is particularly important when improving the estimation accuracy of the scaling exponent of nonstationary time series. To show this effect, we investigate the scaling behavior estimated by centered and backward DMAs when applied to nonstationary signals with a polynomial trend. In our analysis, the analyzed time series are generated by superposition of white Gaussian noise and a qth degree polynomial function. As shown in Fig. 7, as the DMA order increases, the effect of the polynomial trend is either attenuated or completely removed. Specifically, the fourth-order centered DMA yields excellent results up to the fifth degree polynomial trend. It is analytically shown that centered DMA with even order m can remove the mth degree polynomial trend in the analyzed time series $\{x(i)\}$, or the $(m + 1)$th degree polynomial trend in $\{y(i)\}$ (see Appendix C). In contrast, our numerical results suggest that mth order backward DMA can remove an $(m - 1)$th degree polynomial trend in the analyzed time series $\{x(i)\}$, or an mth degree polynomial trend in $\{y(i)\}$. An analytical proof of this property is also given in Appendix C. Therefore, the zeroth-order backward DMA has poor detrending ability, as shown in Fig. 7(c).

Compared to backward DMA, centered DMA at the same (even) order has better detrending ability. In addition, centered DMA shows better scaling behavior at small scales than backward DMA. Therefore, we recommend centered DMA for scaling analysis, unless there is a strong reason to use backward DMA.

V. APPLICATION OF HIGHER-ORDER DMA

Our algorithm facilitates the application of higher-order DMA to real-world time series. As shown in Fig. 7, undesirable scaling behavior induced by deterministic trends is removed or attenuated by increasing the order of the DMA. In other words, the slope of the desirable scaling behavior is not changed by increasing the order of DMA used. Therefore, to validate the observed scaling behavior, we must demonstrate that the estimated scaling exponent remains unchanged when the order of the DMA is increased.

As an application of centered DMA, here we analyze HRV time series obtained from the Physionet database [37]. Long-term HRV in healthy subjects has been shown to exhibit a $1/f^{\beta}$-type power spectrum, where β is close to unity for young adults; this behavior derives from the intrinsic stochasticity of heart-rate dynamics [16,18]. As shown in Fig. 8, the $1/f$-scaling behavior was confirmed using centered DMA. The estimated scaling exponent in centered DMA was $\alpha \approx 1.1$, independent of the order of DMA used. Note that $\alpha = 1$ for large scales, which is equivalent to $\beta = 1$ for low frequencies, because of the relation $\alpha = (\beta + 1)/2$. When we compare the estimated results obtained using DMA and DFA, the mth order centered DMA yields very similar results to $(m + 1)$th order DFA. This similarity may originate from the similarity of the single-frequency response functions [40].

The total number of heart beats over 24 h is approximately 10^5. Furthermore, in medical cohort studies using 24-h HRV, analysis of a large number datasets would be sometimes required [18]. When analyzing these datasets using higher-order DMA, our algorithm might be useful.

VI. SUMMARY AND DISCUSSION

We have proposed a fast algorithm for higher-order DMA that can significantly reduce the computational cost relative

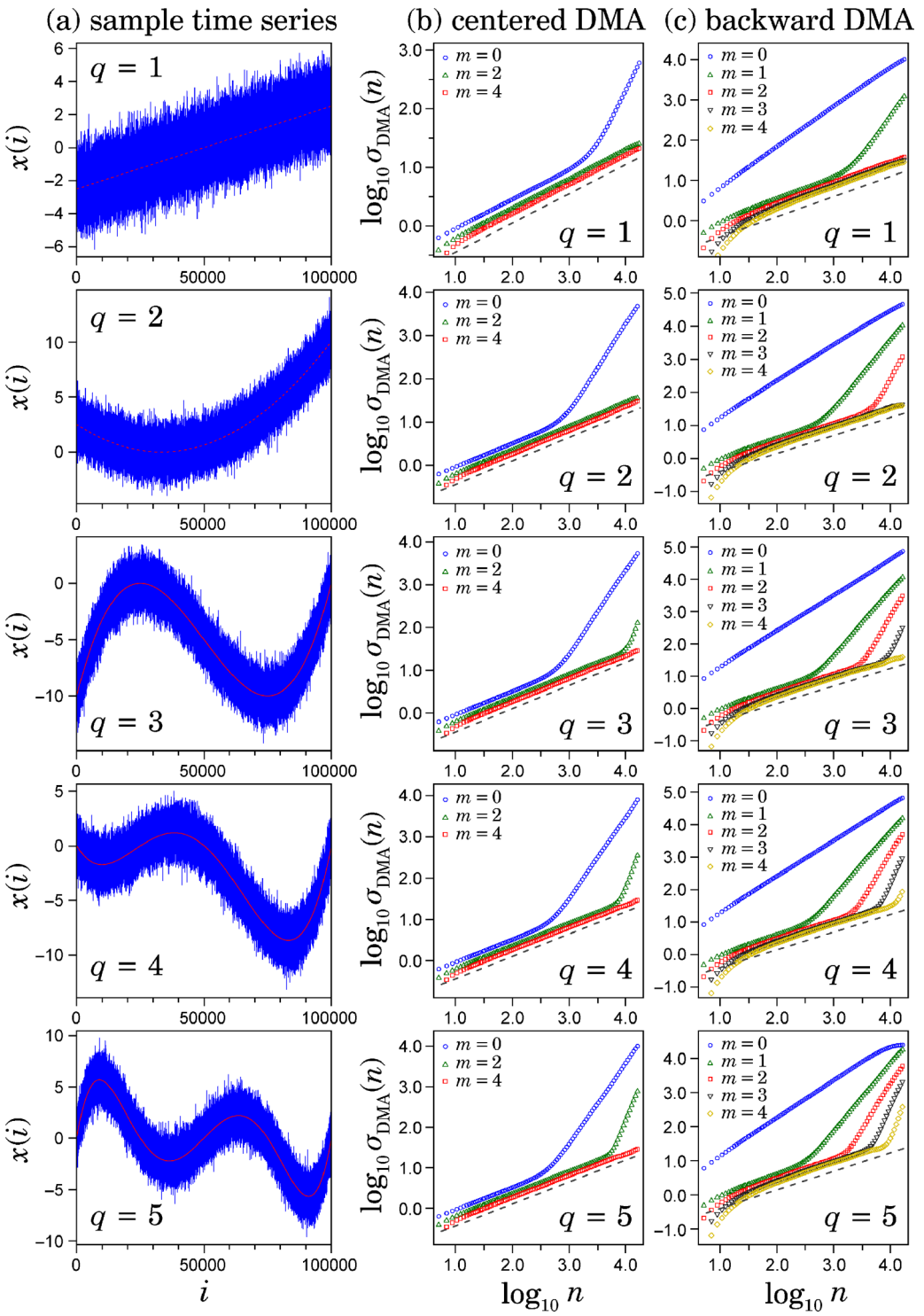

FIG. 7. Detrending capability for removing a polynomial trend. The analyzed time series were generated by superposition of white Gaussian noise and a qth order polynomial function, and analyzed by centered DMA (center) and backward DMA (right). The estimated values of $\sigma_{\mathrm{DMA}}(n)$ for each value of n were averaged over 10 samples. From top to bottom, linear, quadratic, cubic, quartic, and quintic trends were analyzed. The left panels show sample time series, where polynomial functions are described using dashed lines. The dashed lines in the center and right panels indicate lines with slope 0.5.

to the conventional straightforward implementation. Using our algorithm for centered DMA and backward DMA, we have numerically shown the order dependence of detectable scaling exponents and the detrending capability for removing a polynomial trend. These properties are also derived analytically. Centered DMA exhibits better performance than forward DMA or backward DMA with the same (even) order. In practical applications, to validate the observed scaling behavior, it is necessary to demonstrate that the estimated scaling exponent remains unchanged when the order of DMA

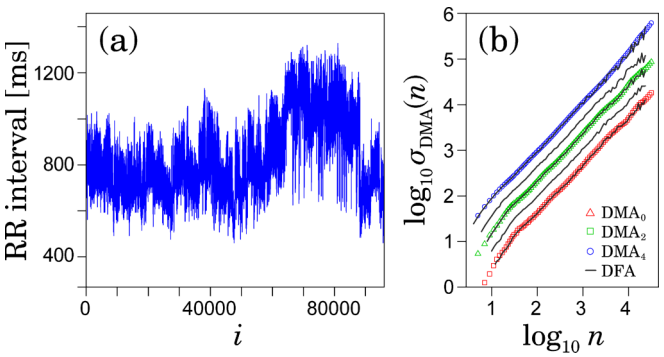

FIG. 8. $1/f$ scaling behavior of heart-rate variability (HRV). (a) HRV time series of a normal subject (a 35-year-old male) [37]. (b) Log-log plots of σ_{DMA} vs. n for centered DMA combined with DFA (solid lines) [25]. In the case of DFA, the fluctuation functions $F(n)$ were plotted instead of σ_{DMA}; In solid lines from top to bottom, the orders of DFA are 1, 2, 3, 4, and 5. The curves have been shifted vertically for better visibility.

is increased. For practical applications, our algorithm for higher-order DMA is an important contribution.

To date, the performance of higher-order DFA has been extensively and systematically studied [41–44], and DFA has become a widely used method. In comparison, studies using higher-order DMA are rare. Our algorithm could help further systematic study of the performance of higher-order DMA and facilitate increasingly widespread application of DMA.

In addition, further extension of higher-order DMA is possible. Zeroth-order DMA with a simple moving average has been extended to higher-dimensional data analysis [45], cross-correlation analysis [46,47], and multifractal analysis [48]. In a similar fashion, by extending our algorithm, higher-order DMA could be extended to a wide range of analysis techniques.

ACKNOWLEDGMENTS

The authors thank Professors Anna Carbone, Taishin Nomura, and Yasuyuki Suzuki for fruitful comments. This work was supported by JSPS KAKENHI, Grant No. 15K01285 and No. 26461094.

APPENDIX A: ALGORITHM FOR BACKWARD DMA

In mth order backward DMA, the mean-square deviation from the trend is given by

$$\sigma^2_{\mathrm{DMA}}(n) = \frac{1}{N-n+1} \sum_{i=1}^{N-n+1} [y(n+i-1) - \tilde{a}_0(i)]^2, \quad \text{(A1)}$$

where $\tilde{a}_0(i)$ is given by

$$\tilde{a}_0(i) = \sum_{k=0}^{m} \tilde{b}_{1,k+1}\, Y^{(k)}(i). \quad \text{(A2)}$$

In Eq. (A2), $Y^{(k)}(i,n)$ is given by

$$Y^{(k)}(i,n) = \sum_{j=1}^{n} (j-n)^k\, y(i+j-1), \quad \text{(A3)}$$

and $\tilde{b}_{i,j}$ is an element of the matrix $B_m^{-1}(n)$, where $B_m^{-1}(n)$ is the inverse matrix of

$$B_m(n) = \sum_{j=-n+1}^{0} \begin{bmatrix} 1 & j & j^2 & \cdots & j^m \\ j & j^2 & j^3 & \cdots & j^{m+1} \\ j^2 & j^3 & j^4 & \cdots & j^{m+2} \\ \vdots & \vdots & \vdots & \ddots & \vdots \\ j^m & j^{m+1} & j^{m+2} & \cdots & j^{2m} \end{bmatrix}. \quad \text{(A4)}$$

In our algorithm, if the condition $i = ri' + 1$ ($i' = 0,1,\cdots$) is satisfied, $Y^{(k)}(i,n_1)$ at the smallest scale n_1 is straightforwardly calculated using Eq. (A3). Otherwise, subsequent $Y^{(k)}(i,n_l)$ values are calculated using recurrence formulas,

$$Y^{(k)}(i+1,n) = \sum_{j=0}^{k} \binom{k}{j} (-1)^{k-j}\, Y^{(j)}(i,n) - (-n)^k\, y(i) + 0^k\, y(i+n). \quad \text{(A5)}$$

Note that in Eq. (A5), we define $0^0 = 1$. In addition, the relation between two scales, n_l and n_{l+1}, is given by

$$Y^{(k)}(i,n_{l+1}) = \sum_{j=0}^{k} \binom{k}{j} (n_l - n_{l+1})^{k-j}\, Y^{(j)}(i,n_l) + \sum_{j=1+n_l}^{n_{l+1}} (j-n_{l+1})^k\, y(i+j-1). \quad \text{(A6)}$$

Therefore, if the two conditions, i.e., $n_l > n_1$ and $i = ri' + 1$, are satisfied, $Y^{(k)}(i,n_l)$ is calculated using Eq. (13).

APPENDIX B: SINGLE-FREQUENCY RESPONSE FUNCTION OF FORWARD AND BACKWARD DMA

Recently, we proposed an analytical approach using the single-frequency response function of DMA [36,40]. The single-frequency response function is obtained by considering the response of DMA for the analysis of a single-frequency component with amplitude A and frequency f. The square root of the single-frequency response function provides an analytical prediction of $\sigma_{\mathrm{DMA}}(n)$ when a single-frequency component is analyzed using DMA. Furthermore, the power-law tail structure of the single-frequency response function for $n \ll 1/f$ determines the upper limit of the scaling exponent detectable by DMA [36,40]. That is, when the single-frequency response function is proportional to n^ν for $n \ll 1/f$, the upper limit of the detectable scaling exponent is equal to $\nu/2$.

In the case of mth order forward DMA and backward DMA, the single-frequency response functions have the same functional form, and, when $n \ll 1/f$, these response functions can be expanded as follows:

$$\overline{\Phi}^2_m(n,f,A) = \frac{\pi^{2m} A^2 f^{2m}}{2^3 \prod_{j=1}^{m} (2j-1)^2}\, n^{2m+2} + O(n^{2m+4}). \quad \text{(B1)}$$

We have analytically confirmed that Eq. (B1) holds when $m = 1,2,\ldots,5$. Therefore, we conjecture that Eq. (B1) holds in general. Hence, in the range where Eq. (B1) holds, the upper

limit of the detectable scaling exponent for mth order forward and backward DMA is equal to $m+1$.

APPENDIX C: ANALYTICAL DERIVATION OF DETRENDING CAPABILITY

When we consider the sum of two uncorrelated time series $\{x^{(A)}(i)\}$ and $\{x^{(B)}(i)\}$, the superposition law of the mean-square deviation in DMA holds [35]:

$$\left[\sigma_{\mathrm{DMA}}^{(A+B)}(n)\right]^2 = \left[\sigma_{\mathrm{DMA}}^{(A)}(n)\right]^2 + \left[\sigma_{\mathrm{DMA}}^{(B)}(n)\right]^2, \tag{C1}$$

where $\sigma_{\mathrm{DMA}}^{(A+B)}(n)$, $\sigma_{\mathrm{DMA}}^{(A)}(n)$, and $\sigma_{\mathrm{DMA}}^{(B)}(n)$ denote the root-mean-square deviation corresponding to $\{x^{(A)}(i)\}$, $\{x^{(B)}(i)\}$, and $\{x^{(A)}(i)+x^{(B)}(i)\}$, respectively. Therefore, if a time series is given by the sum of stochastic noise and a polynomial trend, the additive law of mean-square deviations holds. Therefore, we can study the separate effects of the polynomial trends. Although the detrending ability of zeroth-order DMA has already been shown by Shao *et al.* [35], we consider higher-order DMA.

1. Centered DMA

First, we study the detrending capability of the mth order centered DMA, where m is chosen to be an even number. To simplify the calculation, we assume a qth order polynomial function defined in the range $[-n',n']$, where the scale is given by $n = 2n'+1$:

$$x^{(q)}(i) = c_0 + c_1 i + \cdots + c_q i^q = \sum_{k=0}^{q} c_k\, i^k. \tag{C2}$$

Note that by employing parallel translation, an arbitrary situation when analyzing polynomial functions can be described in this form. In this case, the integrated series in $[-n',n']$ is given by

$$y^{(q)}(i) = \sum_{j=-n'}^{i} x^{(q)}(j) = \sum_{k=0}^{q} c_k \sum_{j=-n'}^{i} j^k. \tag{C3}$$

Using the following expression based on Faulhaber's formula,

$$\sum_{j=-n'}^{i} j^k = \begin{cases} \frac{1}{k+1}\sum_{j=0}^{k}(-1)^j B_j \binom{k+1}{j}\{i^{k+1-j} + (-1)^k (n')^{-j+k+1}\} & \text{for} \quad k \neq 0 \\ i + n' + 1 & \text{for} \quad k = 0 \end{cases}, \tag{C4}$$

where B_j are the Bernoulli numbers. We express $y^{(q)}(i)$ as

$$\begin{aligned} y^{(q)}(i) &= c_0 + \sum_{k=0}^{q} \frac{c_k}{k+1} \sum_{j=0}^{k} (-1)^j B_j \binom{k+1}{j} \{i^{k+1-j} + (-1)^k (n')^{-j+k+1}\} \\ &= c_0 + \sum_{k=0}^{q} \frac{c_k}{k+1} \sum_{j=0}^{k} (-1)^j B_j \binom{k+1}{j} (-1)^k (n')^{-j+k+1} + \sum_{k=0}^{q} \left\{ \sum_{j=k}^{q} \frac{c_j}{j+1} (-1)^{j-k} B_{j-k} \binom{j+1}{j-k} \right\} i^{k+1}. \end{aligned} \tag{C5}$$

As described in Eq. (C5), we can express $y^{(q)}(i)$ as

$$y^{(q)}(i) = \hat{c}_0 + \hat{c}_1\, i + \hat{c}_2\, i^2 + \cdots + \hat{c}_{q+1}\, i^{q+1}. \tag{C6}$$

To calculate the moving average point at $i=0$, we first obtain the coefficients $\{a_k\}$ of the least-squares polynomial by minimizing

$$I(\{a_j\}) = \sum_{i=-n'}^{n'} \left(y^{(q)}(i) - \sum_{k=0}^{m} a_k i^k \right)^2. \tag{C7}$$

That is, we solve the following equations:

$$\frac{\partial I(\{a_j\})}{\partial a_i} = 0, \tag{C8}$$

where $i,j = 0,1,\ldots,m$. When $q \leqslant m$, equations given by Eq. (C8) for even i values result in

$$\begin{bmatrix} \rho_0 & \rho_2 & \cdots & \rho_m \\ \rho_2 & \rho_4 & \cdots & \rho_{m+2} \\ \rho_4 & \rho_6 & \cdots & \rho_{m+4} \\ \vdots & \vdots & & \vdots \\ \rho_m & \rho_{m+2} & \cdots & \rho_{2m} \end{bmatrix} \begin{bmatrix} a_0 - \hat{c}_0 \\ a_2 - \hat{c}_2 \\ a_4 - \hat{c}_4 \\ \vdots \\ a_m - \hat{c}_m \end{bmatrix} = \begin{bmatrix} 0 \\ 0 \\ 0 \\ \vdots \\ 0 \end{bmatrix}, \tag{C9}$$

where

$$\rho_k = \sum_{i=-n'}^{n'} i^k. \tag{C10}$$

Because when $m < 2n'+1$, a unique solution to Eq. (C9) exists, we obtain

$$a_k = \hat{c}_k \quad \text{for} \quad k = 0,2,4,\ldots m. \tag{C11}$$

In this case, the mth order centered moving average at $i=0$ is given by

$$\tilde{y}_n(0) = a_0 = \hat{c}_0. \tag{C12}$$

Therefore, the square deviation at $i=0$ is calculated as

$$[y^{(q)}(i) - \tilde{y}_n(i)]^2|_{i=0} = [\hat{c}_0 - \tilde{y}_n(0)]^2 = 0, \tag{C13}$$

which means that when $q \leqslant m$, the mth order moving average coincides with the $(q+1)$th order polynomial function $y^{(q)}(i)$. In other words, this result demonstrates that $\sigma^2_{\mathrm{DMA}}(n) = 0$ when the qth order polynomial function $x^{(q)}(i)$ for $q \leqslant m$ is analyzed using mth order centered DMA. On the other hand, when $q > m$, the square deviations from the trend take nonzero

values. For instance, when $m = 2$ and $q = 3$, we obtain

$$\sigma^2_{\mathrm{DMA}}(n) = \frac{9\,c_3^2(n^4 - 10n^2 + 9)^2}{5017600} \sim n^8, \tag{C14}$$

and when $m = 4$ and $q = 5$, we obtain

$$\sigma^2_{\mathrm{DMA}}(n) = \frac{25\,c_5^2(n^6 - 35n^4 + 259n^2 - 225)^2}{7\,868\,399\,616} \sim n^{12}. \tag{C15}$$

2. Backward DMA

Next, we study the detrending capability of mth order backward DMA. In this case, we consider a qth order polynomial function $x^{(q)}(i)$ [Eq. (C2)] defined in the range $[-n+1,0]$. In this range, the integrated series $y_n(i)$ is given by

$$y^{(q)}(i) = \sum_{j=-n+1}^{i} x^{(q)}(j) = \hat{c}_0 + \hat{c}_1\, i + \hat{c}_2\, i^2 + \cdots + \hat{c}_{q+1}\, i^{q+1}, \tag{C16}$$

where

$$\hat{c}_0 = c_0 + \sum_{k=0}^{q} \frac{c_k}{k+1} \sum_{j=0}^{k} (-1)^j B_j \binom{k+1}{j} (-1)^k (n-1)^{-j+k+1},$$

$$\hat{c}_{k+1} = \sum_{j=k}^{q} \frac{c_j}{j+1} (-1)^{j-k} B_{j-k} \binom{j+1}{j-k} \quad \text{for} \quad k = 0, \ldots, q.$$

To minimize

$$I(\{a_j\}) = \sum_{i=-n+1}^{0} \left(y^{(q)}(i) - \sum_{k=0}^{m} a_k i^k \right)^2, \tag{C17}$$

we solve

$$\begin{bmatrix} \rho_0 & \rho_1 & \cdots & \rho_m \\ \rho_1 & \rho_2 & \cdots & \rho_{m+1} \\ \rho_2 & \rho_3 & \cdots & \rho_{m+2} \\ \vdots & \vdots & \ddots & \vdots \\ \rho_m & \rho_{m+1} & \cdots & \rho_{2m} \end{bmatrix} \begin{bmatrix} a_0 - \hat{c}_0 \\ a_1 - \hat{c}_1 \\ a_2 - \hat{c}_2 \\ \vdots \\ a_m - \hat{c}_m \end{bmatrix} = \begin{bmatrix} 0 \\ 0 \\ 0 \\ \vdots \\ 0 \end{bmatrix}, \tag{C18}$$

where

$$\rho_k = \sum_{i=-n+1}^{0} i^k, \tag{C19}$$

and thus obtain

$$a_k = \hat{c}_k \quad \text{for} \quad k = 0,1,2,\ldots m. \tag{C20}$$

In this case, the backward moving average at $i = 0$ is given by

$$\tilde{y}_n(0) = a_0 = \hat{c}_0. \tag{C21}$$

Therefore, the square deviation at $i = 0$ is calculated as $[\hat{c}_0 - \tilde{y}_n(0)]^2 = 0$. This result indicates that when $q \leqslant m - 1$, the mth order moving average coincides with the qth order polynomial function $y^{(q)}(i)$, and $\sigma^2_{\mathrm{DMA}}(n) = 0$. On the other hand, when $q > m - 1$, the square deviations from the trend take nonzero values. For example, when $m = 2$ and $q = 2$, we obtain

$$\sigma^2_{\mathrm{DMA}}(n) = \frac{c_2^2\,(n-3)^2\,(n-2)^2\,(n-1)^2}{3600} \sim n^6. \tag{C22}$$

Based on the same approach, it is possible to show that the detrending capability of forward DMA is the same as that of backward DMA.

[1] M. Kobayashi and T. Musha, IEEE Trans. Biomed. Eng. **BME-29**, 456 (1982).
[2] C.-K. Peng, J. Mietus, J. M. Hausdorff, S. Havlin, H. E. Stanley, and A. L. Goldberger, Phys. Rev. Lett. **70**, 1343 (1993).
[3] C.-K. Peng, S. V. Buldyrev, S. Havlin, M. Simons, H. E. Stanley, and A. L. Goldberger, Phys. Rev. E **49**, 1685 (1994).
[4] C.-K. Peng, S. Havlin, H. E. Stanley, and A. L. Goldberger, Chaos **5**, 82 (1995).
[5] J. M. Hausdorff, P. L. Purdon, C. K. Peng, Z. Ladin, J. Y. Wei, and A. L. Goldberger, J. Appl. Physiol. **80**, 1448 (1996).
[6] K. Kiyono, Z. R. Struzik, N. Aoyagi, F. Togo, and Y. Yamamoto, Phys. Rev. Lett. **95**, 058101 (2005).
[7] R. N. Mantegna and H. E. Stanley, *Introduction to Econophysics: Correlations and Complexity in Finance* (Cambridge University Press, Cambridge, 1999).
[8] J. Alvarez-Ramirez, E. Rodriguez, and J. C. Echeverría, Physica A **354**, 199 (2005).
[9] Y. Wang, Y. Wei, and C. Wu, Physica A **390**, 864 (2011).
[10] D. Rybski, S. V. Buldyrev, S. Havlin, F. Liljeros, and H. A. Makse, Proc. Natl. Acad. Sci. USA **106**, 12640 (2009).
[11] C. Fan, J.-L. Guo, and Y.-L. Zha, Physica A **391**, 6617 (2012).
[12] H. Takayasu, *Fractals in the Physical Sciences* (Manchester University Press, Manchester, 1990).
[13] D. Sornette, *Critical Phenomena in Natural Sciences: Chaos, Fractals, Selforganization and Disorder* (Springer, Berlin, 2006).
[14] S. Madden, IEEE Internet Comput. **16**, 4 (2012).
[15] J. Andreu-Perez, C. C. Poon, R. D. Merrifield, S. T. Wong, and G.-Z. Yang, IEEE J. Biomed. Health Inform. **19**, 1193 (2015).
[16] T. Nakamura, K. Kiyono, H. Wendt, P. Abry, and Y. Yamamoto, Proc. IEEE **104**, 242 (2016).
[17] M. Baumert, V. Baier, and A. Voss, Fluc. Noise Lett. **05**, L549 (2005).
[18] R. Sassi, S. Cerutti, F. Lombardi, M. Malik, H. V. Huikuri, C.-K. Peng, G. Schmidt, Y. Yamamoto, B. Gorenek, G. H. Lip *et al.*, Europace **17**, 1341 (2015).
[19] G. Rangarajan and M. Ding, Phys. Rev. E **61**, 4991 (2000).
[20] H. E. Hurst, Trans. Amer. Soc. Civil Eng. **116**, 770 (1951).
[21] C. Peng, S. Buldyrev, A. Goldberger, S. Havlin, F. Sciortino, M. Simons, H. Stanley *et al.*, Nature **356**, 168 (1992).

[22] M. Holschneider, J. Stat. Phys. **50**, 963 (1988).
[23] D. Veitch and P. Abry, IEEE Trans. Inf. Theory **45**, 878 (1999).
[24] J.F. Muzy, E. Bacry, and A. Arneodo, Phys. Rev. Lett. **67**, 3515 (1991).
[25] J. W. Kantelhardt, E. Koscielny-Bunde, H. H. Rego, S. Havlin, and A. Bunde, Physica A **295**, 441 (2001).
[26] N. Vandewalle and M. Ausloos, Phys. Rev. E **58**, 6832 (1998).
[27] E. Alessio, A. Carbone, G. Castelli, and V. Frappietro, Eur. Phys. J. B **27**, 197 (2002).
[28] A. Carbone, G. Castelli, and H. E. Stanley, Phys. Rev. E **69**, 026105 (2004).
[29] B. B. Mandelbrot and J. W. Van Ness, SIAM Rev. **10**, 422 (1968).
[30] C. Chianca, A. Ticona, and T. Penna, Physica A **357**, 447 (2005).
[31] A. Bashan, R. Bartsch, J. W. Kantelhardt, and S. Havlin, Physica A **387**, 5080 (2008).
[32] X.-Y. Qian, G.-F. Gu, and W.-X. Zhou, Physica A **390**, 4388 (2011).
[33] S. Arianos, A. Carbone, and C. Türk, Phys. Rev. E **84**, 046113 (2011).
[34] Y.-H. Shao, G.-F. Gu, Z.-Q. Jiang, W.-X. Zhou, and D. Sornette, Sci. Rep. **2** 535 (2012).
[35] Y.-H. Shao, G.-F. Gu, Z.-Q. Jiang, and W.-X. Zhou, Fractals **23**, 1550034 (2015).
[36] A. Carbone and K. Kiyono, arXiv:1602.01260.
[37] A. L. Goldberger, L. A. Amaral, L. Glass, J. M. Hausdorff, P. C. Ivanov, R. G. Mark, J. E. Mietus, G. B. Moody, C.-K. Peng, and H. E. Stanley, Circulation **101**, e215 (2000).
[38] A. Savitzky and M. J. Golay, Anal. Chem. **36**, 1627 (1964).
[39] M. U. Bromba and H. Ziegler, Anal. Chem. **55**, 1299 (1983).
[40] K. Kiyono, Phys. Rev. E **92**, 042925 (2015).
[41] K. Hu, P. C. Ivanov, Z. Chen, P. Carpena, and H. E. Stanley, Phys. Rev. E **64**, 011114 (2001).
[42] Z. Chen, P. C. Ivanov, K. Hu, and H. E. Stanley, Phys. Rev. E **65**, 041107 (2002).
[43] Z. Chen, K. Hu, P. Carpena, P. Bernaola-Galvan, H. E. Stanley, and P. C. Ivanov, Phys. Rev. E **71**, 011104 (2005).
[44] Q. D. Y. Ma, R. P. Bartsch, P. Bernaola-Galván, M. Yoneyama, and P. C. Ivanov, Phys. Rev. E **81**, 031101 (2010).
[45] A. Carbone, Phys. Rev. E **76**, 056703 (2007).
[46] S. Arianos and A. Carbone, J. Stat. Mech. (2009) P03037.
[47] L. Kristoufek, Physica A **406**, 169 (2014).
[48] G.-F. Gu and W.-X. Zhou, Phys. Rev. E **82**, 011136 (2010).